Dynamics Calculations on Bis(hydrazine) and Bis(hydrazyl) Radical Cation Intramolecular Electron Transfer

Stephen F. Nelsen

Contribution from the S. M. McElvain Laboratories of Organic Chemistry, Department of Chemistry, University of Wisconsin, 1101 West University Avenue, Madison, Wisconsin 53706-1396

Received July 28, 1995[⊗]

Abstract: Bis(hydrazine) **[22/HEX/22]** exists principally in the unsymmetrical double nitrogen inversion form at 230 K. UHF/AM1 dynamics calculations starting from the radical cation of the above material and syn and anti **[B/TET/B]**$^+$, each constrained to have equivalent dinitrogen units so they represent the electron transfer transition states, indicate that many modes (10 or more) contribute to reaching the electron transfer transition state, and that the frequencies involved are predictable from those of the relaxed radical cations. The results were analyzed to give average barrier-crossing frequencies activated at the transition state for electron transfer ($\langle h\nu_{in}\rangle$) of 827, 1403, and 1293 cm^{-1}, respectively. A V of 5.0 kcal/mol was obtained from the experimental data for **[22/HEX/22]**$^+$ when used with the first-order adiabatic energy surface expression (text eq 4), and of 4.7 at $\langle h\nu_{in}\rangle$ = 827 cm^{-1} using Jortner's single averaged vibronic coupling treatment (text eq 6). These V values are between that estimated using Hush theory on the CT band (3.9 kcal/mol) and that obtained by AM1 calculations (6.1 kcal/mol). The Holstein tunneling coefficient expression (text eq 7) gives poor fit to our data, but better fit is attained using a multiple mode fit with a Hush equation (text eq 10) which employs a preexponential factor for $\Gamma(q)$ which makes tunneling of increasing importance as the number of modes increases, and high-frequency modes contribute significantly even when they have tiny contributions to the barrier.

Introduction

This work concerns electron transfer (ET) rate studies of compounds containing bis(*N*,*N*′-bicyclic) hydrazine **[22/22]^0** and *tert*-butyldiazabicyclooctenyl cation **[22/B]**$^+$ units. One-electron

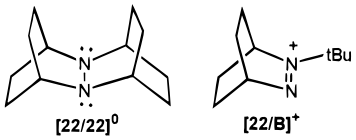

oxidation of the former and one-electron reduction of the latter produce long-lived 3e−π bonded NN-centered radicals. These dinitrogen units have been doubly linked by four σ-bonds between the nitrogens to give dimeric species, prepared from the bis(azo) compounds **HEX** or **TET** (the abbreviations stand

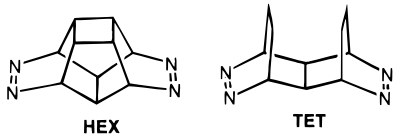

for the number of rings in the azo compounds). The dimer radical cations may be considered organic intervalence compounds because they have their charge and spin instantaneously localized on one NN unit. They exhibit charge-transfer (CT) bands analogous to those of transition metal intervalence compounds,[1] which are useful for considering the rate of ET between the units, as Hush has pointed out.[2] Solvent effect studies on CT band maxima (E_{op}, which is equal to Marcus's vertical ET energy difference λ) for intervalence compounds allow experimental determination of both λ_{in} and λ_{out}.[2,3] Optical studies on the radical cations derived from the bis(diazenium) dications syn and anti **[B/TET/B]**$^+$, as well as their *N*-methyl hydrazine analogues, have been reported previously.[4] The bis(diazenium) radical cation CT maxima appear in the near-IR

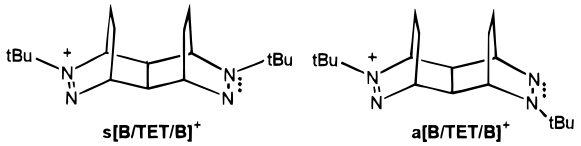

and those of the bis(hydrazines) in the visible, showing that λ is far higher for the bis(hydrazine) radical cations. Calculations were helpful in understanding the λ values. If **n** and **c** represent the relaxed geometries of neutral and cationic forms of a hydrazine unit and the charges are shown as superscripts, the precursor pair is **n^0**,**c**$^+$, the vertical ET pair is **n**$^+$,**c^0**, and λ_{in} is the free energy difference between them. The enthalpy portion of λ_{in}, which we will call λ_{in}', is easily calculated using AM1;[6] λ_{in}' may be expressed as shown in (1a) and (1b) for dimeric bis(hydrazine) and bis(diazenium) radical cations respectively.

[⊗] Abstract published in *Advance ACS Abstracts,* February 1, 1996.

(1) For a review of intervalence complexes, see: Creutz, C. *Prog. Inorg. Chem.* **1983**, *30*, 1.

(2) (a) Hush, N. S. *Trans. Faraday Soc.* **1961**, 57, 557. (b) Allen, G. C.; Hush, N. S. *Prog. Inorg. Chem.* **1967**, *8*, 357, 391. (c) Hush, N. S. *Coord. Chem. Rev.* **1985**, *64*, 135. (d) Hush, N. S. In *Mixed Valence Compounds*; Brown, D. B., Ed.; Reidel: Dordrecht, The Netherlands, 1980; p 151.

(3) (a) Marcus, R. A.; Sutin, N. *Biochim. Biophys. Acta* **1985**, *811*, 265−322. (b) Sutin, N. *Prog. Inorg. Chem.* **1983**, *30*, 441. (c) It is frustrating to keep the nomenclature straight because even the same author frequently changes what he calls various quantities. What we call λ_{out} here is often called λ_s, $\lambda_{in} \rightarrow \lambda_v$, $\lambda \rightarrow \chi$ or E_λ, $V \rightarrow H_{ab}$ or J, and $h\nu \rightarrow \hbar\omega$. Most formulas are also often written with $R \rightarrow k_B$.

(4) Nelsen, S. F.; Chang, H.; Wolff, J. J.; Adamus, J. *J. Am. Chem. Soc.* **1993**, *115*, 12276.

(5) Nelsen, S. F.; Adamus, J.; Wolff, J. J. *J. Am. Chem. Soc.* **1994**, *116*, 1589.

(6) (a) Nelsen, S. F.; Blackstock, S. C.; Kim, Y. *J. Am. Chem. Soc.* **1987**, *109*, 677. (b) Nelsen, S. F. Internal Geometry Relaxation Effects on Electron Tranfer Rates of Amino Centered System. In *Advances in Electron Transfer Chemistry*; Mariano, P. S., Ed.; JAI: Greeenwich, CT, 199X; Vol. 3.

0002-7863/96/1518-2047$12.00/0

Scheme 1

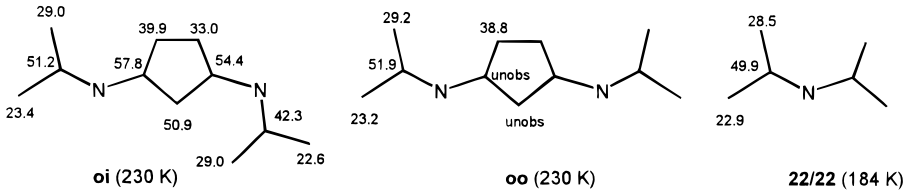

UHF/AM1 calculations of λ_{in}' gave values which were consistent with the CT maximum data, and differences in E_{op} between the

$$\lambda_{in}' = [\Delta H_f(\mathbf{n}^+) - \Delta H_f(\mathbf{n}^0)] + [\Delta H_f(\mathbf{c}^0) - \Delta H_f(\mathbf{c}^+)] = \Delta H_{rel}(\mathbf{n}) + \Delta H_{rel}(\mathbf{c}) \quad (1a)$$

$$\lambda_{in}' = [\Delta H_f(\mathbf{d}^+) - \Delta H_f(\mathbf{d}^{2+})] + [\Delta H_f(\mathbf{c}^{2+}) - \Delta H_f(\mathbf{c}^+)] = \Delta H_{rel}(\mathbf{d}) + \Delta H_{rel}(\mathbf{c}) \quad (1b)$$

bis(hydrazines) and the bis(diazenes) were close to the differences in calculated λ_{in}'. Because λ_{out} should be the same for molecules so similar in structure, it appeared that the calculations successfully predicted λ_{in} for both classes of compounds. Unfortunately, the intramolecular electron exchange rate constants k_{ex} for these compounds fall outside the range experimentally measurable by dynamic ESR. The bis(diazeniums) have k_{ex} too large to measure even at −100 °C, and the bis(hydrazines) have k_{ex} too small to measure even at +75 °C.[4] Although this was consistent with the λ values obtained from the optical studies, it precluded quantitative testing of theory. We next studied bis(hydrazine) radical cation **[22/HEX/22]**$^+$, calculated to have smaller λ_{in} and hence larger k_{ex}.[5] It proved

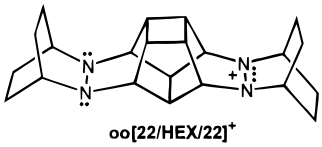

oo[22/HEX/22]$^+$

to have a k_{ex} value which is ideal for dynamic ESR studies; the temperature of maximum broadening, where greatest accuracy is attained, is near room temperature. These studies gave $k_{ex}(298K,CH_3CN) = 1.3_2 \times 10^8\ s^{-1}$ and an anomalously small temperature effect; $k_{ex}(350K)/k_{ex}(250K) = 2.0$,[5] far smaller than expected. High λ_{in} is necessary to make k_{ex} small enough to measure for cases with reasonably large V, and symmetrical transition metal-centered cases are predicted to have k_{ex} too large to measure. The solvent study on E_{op} for **[22/HEX/22]**$^+$ gave vertical barriers $\lambda_{in} = 37.6$ kcal/mol and $\lambda_{out} = 9.0$ kcal/mol. For **oo**$^+$**[22/HEX/22]**$^+$ $\lambda_{in}' = 34.3$ kcal/mol is calculated, 88% as large as the experimental λ_{in} value. The special geometry constraints of these *N*,*N*′-bis(bicyclic) structures are required to make AM1 calculations give good estimates of λ_{in}'; AM1 calculations give far poorer estimates for other types of hydrazines.[7]

Two other types of parameters are required for calculation of k_{ex}, which would actually allow comparison of the observed rate constant with theory. The frequencies $h\nu_{in}$, which carry the system through the ET transition state, and the electronic matrix coupling element V, which is half the energy separation of the ground and excited state surfaces at the transition state, are also needed. This paper is principally concerned with using UHF/AM1 calculations to consider nitrogen pyramidality influences on λ_{in}', estimating $h\nu_{in}$ and V values, and the comparison of calculated parameters with the experimental rate constant for **[22/HEX/22]**$^+$.

(7) Nelsen, S. F.; Wang, Y.; Powell, D. R.; Hiyashi, R. K. *J. Am. Chem. Soc.* **1993**, *115*, 5246.

Conformations of [22/HEX/22]^0

The link between the hydrazine units has two faces, so each unit can exist in two double nitrogen inversion forms (invertomers). We shall call the invertomer which places the dimethylene bridges syn to the four-membered ring **o** (for "out"), and the other one **i** (for "in"). The invertomer illustrated above for the cation is **oo**, calculated to be the most stable one for the neutral compound by both molecular mechanics and semiempirical methods. MM2 calculations get **io** 0.83 kcal/mol higher in steric energy and **ii** 2.03 kcal/mol higher, while AM1 calculations, which underestimate invertomer energy differences in 2,3-diazabicyclooctane derivatives,[7] get the same order with 0.34 and 1.34 enthalpy differences. These predictions prove incorrect. **[22/HEX/22]**^{0} shows only one carbon peak which is narrow enough to observe at room temperature, at 51.53 δ. Cooling to 230 K gives a major set of 11 sharp signals which can only correspond to the unsymmetrical **io**/**oi** invertomer. A much weaker set of 4 signals is also observed, which we presume are the **oo** invertomer; signals for the half-intensity central carbons and the N*C* in the central portion of the molecule were not observed. Scheme 1, which also shows the signals for "frozen" **22/22**,[8] gives assignments based upon the variable temperature study described below. The minor **oo** invertomer has peak heights ≤20% of the **io** signals, so it consitutes ≤10% of the equilibrium mixture, corresponding to $\Delta G°$ for its formation of ≥1.0 kcal/mol. The **oi**/**io** invertomer mixture is favored by a mixing entropy of 0.3 kcal/mol at 230 K, and it is clearly lower in $\Delta H°$ than **oo**. Obviously, both types of calculations fail to predict which invertomer is the more stable, for reasons that are not apparent. MM2 and AM1 calculations also get invertomer relative energies wrong for certain other neutral hydrazines, as discussed elsewhere.[7]

The single peak observed at room temperature must correspond to the central carbons, which do not move when two double N inversions interconvert **io** with **oi**. At 320 K, in addition to this signal (at 51.7 δ, 0.8 δ downfield of its position at 230 K), a still broad peak centered at 56.9 δ corresponding to the link N*C* carbons (0.8 δ downfield of the average of these signals at 230 K, where $\Delta\delta_{230}$ is 3.39) is clearly growing in, and very broad absorption is observed at 27 ± 0.7 δ, corresponding to the methylene carbon signals ($\Delta\delta_{230} \cong 5.65$ and 6.50) begining to sharpen. The other interconverting pairs have even larger $\Delta\delta_{230}$ values (6.91 for the cyclobutane carbons and 8.97 for the **22** ring N*C* signals) and have not yet sharpened enough to observe. **22/22** undergoes double N inversion with $T_c(25MHz) = 218$ K, and has $\Delta G^{\ddagger}_N = 10.4$ kcal/mol.[9] As discussed elsewhere,[7] the anti lone pair form is an unobserved intermediate in double nitrogen inversion of **22/22**, so the rate limiting step is presumably the barrier for single nitrogen

(8) Nelsen, S. F.; Frigo, T. B.; Kim, Y.; Thompson-Colón, J. A. *J. Am. Chem. Soc.* **1986**, *108*, 7926.

(9) Nelsen, S. F.; Blackstock, S. C.; Haller, K. J. *Tetrahedron* **1986**, *42*, 6101.

Table 1. Summary of AM1 Calculations[a] on the Hydrazines and Diazeniums Discussed Here

species	sym	$\Delta\Delta H_f$[b]	α_{av}[c]	ΔH_f(vert)	λ'_{in}
hydrazines					
[22/22]^0	C_s	29.64	113.2 {*112.8*}	196.75	
[22/22]$^+$	C_{2v}	181.39	118.1 {*118.3*}	47.48	33.20
oo[22/HEX/22]^0	C_{2v}	121.40 {*0.00*}	113.1	289.35	
oi[22/HEX/22]^0	C_s	121.73 {*0.33*}	113.1, 113.3	288.45	
ii[22/HEX/22]^0	C_{2v}	122.74 {*1.74*}	113.3	290.19	
oo[22/HEX/22]$^+$	C_s	273.98 {*0.42*}	113.2, 118.2	140.30	34.29
oi$^+$[22/HEX/22]$^+$	C_s	273.56 {*0.00*}	113.2, 118.0	139.30	32.46
$^+$oi[22/HEX/22]$^+$	C_s	275.27 {*1.71*}	113.5, 118.1	140.39	31.74
ii$^+$[22/HEX/22]$^+$	C_s	275.41 {*1.85*}	113.6, 118.1	140.66	32.70
oo[22/HEX/22]$^{+\ddagger}$	C_{2v}	281.87	115.4		
diazeniums					
[22/B]$^+$	C_1	181.47	120.0	35.05	
[22/B]^0	C_1	27.74	117.8	192.12	17.97
s[B/TET/B]$^{2+}$	C_s	471.32	120.0	256.76	
(o)s[B/TET/B]$^+$	C_1	248.51	118.1, 120.0	481.54	18.47
(i)s[B/TET/B]$^+$	C_1	249.29	118.9, 120.0	481.10	17.25
s[B/TET/B]$^{+\ddagger}$	C_s	252.47	120.0		
a[B/TET/B]$^{2+}$	C_2	470.38	120.0	256.03	
(o)a[B/TET/B]$^+$	C_1	247.96	120.0, 118.2	480.46	18.15
(i)a[B/TET/B]$^+$	C_1	248.58	120.0, 118.9	479.94	17.07
a[B/TET/B]$^{+\ddagger}$	C_2	251.75	120.0		

[a] UHF/AM1 was used for open-shell species (hydrazine radical cations and neutral hydrazyls). [b] The numbers in curley brackets show $\Delta\Delta H_f$ values relative to the most stable invertomer. [c] Numbers in italics are X-ray crystallographic values (from ref 5).

inversion to produce an anti intermediate. The link N*C* carbons of **[22/HEX/22]** have T_c(90MHz) of 300 ± 10 K, corresponding to $\Delta G^{\ddagger}_N(300\pm10) = 13.2\ (\pm0.5_6)$ kcal/mol. More difficult flattening at nitrogen in **[22/HEX/22]** than in **22/22** is also indicated by the standard potential for oxidation of the dimeric compound being 2.1 kcal/mol more difficult,[5] although effects transmitted through the link may also contribute to this difference.[4] The differences are induced by the presence of the hexacyclic link, although because our calculations get the relative energies of **oi** and **oo** wrong, any attempt at detailed consideration of why this occurs seems unwise.

Conformations of [22/HEX/22]$^+$

X-ray crystallographic structures of the hydrazine "monomers" **22/22^0** and **22/22$^+$** have established that both the oxidized and reduced hydrazine units are pyramidalized, with the oxidized unit significantly closer to being planar.[8] Geometry optimization of **oo[22/HEX/22]$^+$** using UHF/AM1 calculations gives a C_s structure with one **22/22** unit near the geometry of the neutral form, and the other near that of the radical cation. UHF/AM1 calculations get the relative energies for the four invertomers of the radical cation shown in Table 1, although the fact that they get the most stable invertomer of the neutral form wrong shows that the calculated enthalpy order may not be right. It may be noted that UHF/AM1 gets invertomers with **o** neutral hydrazine units ≥1.3 kcal/mol more stable than those with **i** units, which is considerably more than the 0.34 **oo** is favored relative to **oi** when both units are neutral. Unfortunately, attempts at getting crystals of **[22/HEX/22]$^+$** fail because it disproportionates. Concentration of the blue solution containing **[22/HEX/22]$^+$** causes colorless neutral and reddish brown dication to precipitate, but unfortunately neither has been obtained as X-ray quality crystals.

Effect of Nitrogen Pyramidality on λ_{in}

It will be noted from Table 1 that λ_{in}' for **[22/HEX/22]$^+$** is rather sensitive to which invertomer is calculated. The reason for this sensitivity is shown in the plot of λ_{in}' versus nitrogen pyramidality for the neutral hydrazine unit **o** invertomers (Figure 1, the plot for the neutral hydrazine unit **i** invertomers, is similar in appearance). We use $\Delta\alpha_{av} = 120 - \alpha_{av}$ to describe

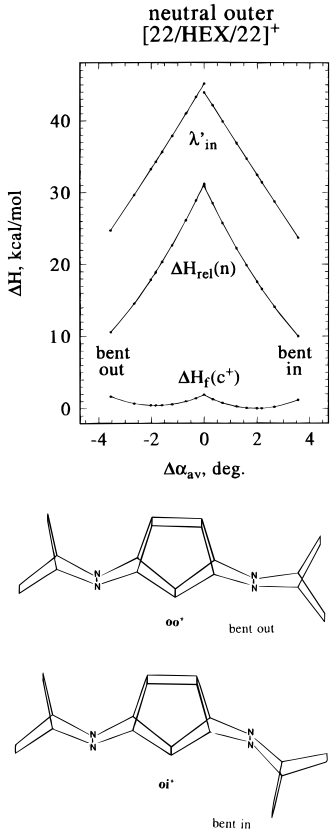

Figure 1. λ_{in}', ΔH_{rel}(**n**), and ΔH_f(**c**$^+$) vs $\Delta\alpha_{av}$ for both invertomers at the oxidized hydrazine unit for **[22/HEX/22]$^+$** pyramidalized outer at the neutral unit.

pyramidality at the oxidized hydrazine unit, and have chosen to use a negative sign for **o** pyramidalization and positive sign for **i** nitrogen pyramidalization. Because the neutral hydrazine unit is strongly bent, ΔH_{rel}(**n**) becomes higher as the oxidized hydrazine unit gets more planar, and this effect dominates λ_{in}', although differences in ΔH_{rel}(**c**) arising from the relative ΔH_f(**c**$^+$) values are also present. Figure 1 emphasizes that in order to get λ_{in}' close to right, the correct pyramidality at nitrogen must be calculated. We note that the **i**$^+$ and **o**$^+$ invertomers

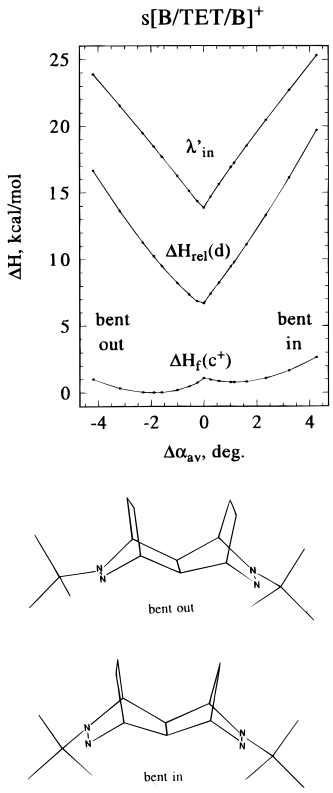

Figure 2. λ_{in}', ΔH_{rel}(**n**), and ΔH_f($\mathbf{c}^+$) vs $\Delta\alpha_{av}$ for both invertomers at the reduced diazenium unit for **s[B/HEX/B]**$^+$.

should have quite similar energies and therefore will be present in comparable amounts. If their λ_{in} values differed significantly, two CT bands would be seen. For example, if the **oi**$^+$ invertomer had the 1.8 kcal/mol lower λ_{in} than the **oo**$^+$ invertomer which is calculated, their absorption maxima would differ by 25 nm. However, even if λ were somewhat lower for **oi**$^+$ than **oo**$^+$, intramolecular ET within **oo**$^+$ would still be more rapid, because that within **oi**$^+$ would be endothermic (1.7 kcal/mol is the calculated endothermicity). Double nitrogen inversion in **22/22**$^+$ is extremely rapid,[6] and an **oi**$^+ \rightarrow$ **oo**$^+$ conversion preceding ET would not limit the rate relative to the observed $k_{ex} = 1.3 \times 10^8$ s^{-1} even if it were required prior to ET. In contrast, inversion at the neutral hydrazine unit is far too slow for it precede the ET process observed. We will only consider calculations on ET within **oo[22/HEX/22]**$^+$ for comparison with experiment for the rest of this paper, and will no longer write the "**oo**".

λ_{in}' of **[B/TET/B]**$^+$ is also sensitive to invertomer at the reduced dinitrogen unit, but because the oxidized unit has a planar nitrogen, the λ_{in}' vs $\Delta\alpha_{av}$ plot has minimum λ_{in}' at $\Delta\alpha_{av} = 0$, as shown in Figure 2. The different shapes of the λ_{in}' vs $\Delta\alpha_{av}$ plots of Figures 1 and 2 appear to have a consequence already observed but not previously understood. All three bis(diazenium) cations studied have an ill-resolved low-energy shoulder which moves with the main band as solvent is changed, so the shoulder appeared to be "part of the CT band".[4] It appears likely that this shoulder represents the CT band for the less stable invertomer at the neutral dinitrogen unit. Pyramidalization will be easier in one direction than the other (**o** pyramidalization is calculated to be easier by AM1) and the more stable invertomer is calculated to be more pyramidal ($\Delta\alpha_{av}$ further from zero) than the less stable one, so both ΔH_f($\mathbf{c}^+$) and ΔH_f($\mathbf{c}^{2+}$) will be larger for the less stable invertomer. Oxidized diazenium units have planar nitrogens so both $\mathbf{c}^+$ invertomers have the same ΔH_f($\mathbf{d}^{2+}$) and ΔH_f($\mathbf{d}^+$) values in eq 1b for the λ_{in}' calculation, and both ΔH_{rel}(**d**) and ΔH_{rel}(**c**) are smaller for the less stable isomer. The AM1 calculations only predict 1.2 and 1.1 kcal/mol smaller λ_{in}' for the less stable (**i**) invertomer of **s**- and **a[B/TET/B]**$^+$, respectively, but it appears from the ill-resolved shoulder on the experimental optical absorption curves that $\Delta\lambda$ is probably closer to 5−7 kcal/mol. It seems clear from Figure 2 that slightly greater pyramidality for the (**o**) form would lead to greater $\Delta\lambda_{in}'$, and that AM1 could not be expected to produce $\Delta\alpha_{av}$ values close enough to the real values to calculate $\Delta\lambda_{in}'$ very accurately. A shoulder was not obtained for **[22/HEX/22]**$^+$. Several factors might contribute to this experimental result. E_{op} is larger (a $\Delta\lambda_{in}$ of 3.0 kcal/mol at 26.5 kcal/mol corresponds to an ΔE_{op} of 122 nm, but at 46.5 kcal/mol to 40 nm), a smaller $\Delta\Delta H_f$($\mathbf{c}^+$) is calculated for the two invertomers which might well lead to less difference in $\Delta\alpha_{av}$, the neutral reference compounds for calculation of λ_{in}' using (1a) are different for the two invertomers of a bis(hydrazine) so the curves do not meet at $\Delta\alpha_{av} = 0$ as they do for bis(diazeniums), and the $\Delta\Delta H_{rel}$(**c**) and $\Delta\Delta H_{rel}$(**n**) effects subtract from each other for hydrazines.

Dynamics Calculations of $h\nu_{in}$

Because AM1 calculations do a surprisingly good job of calculating λ_{in} for the compounds considered here, we hoped that they might be able to estimate the modes giving rise to λ_{in} reasonably well. We used essentially the same method as Rauhaut and Clark employed for intermolecular cases between tetramethyl-*p*-phenylenediamine and its radical cation.[10] For our intramolecular cases, restricting both dinitrogen units to the same geometry by enforcing symmetry (C_{2v} for **[22/HEX/22]**$^+$, C_s for **s[B/TET/T]**$^+$, and C_2 for **a[B/TET/B]**$^+$) gives structures suitably higher in ΔH_f than the relaxed, unsymmetrical structures, which we argue are useful models for the ET transition states of these systems. For example, C_{2v} **[22/HEX/22]**$^{+\ddagger}$ lies 7.9 kcal/mol higher in ΔH_f than the relaxed (C_s) ground state. UHF/AM1 dynamic reaction coordinate (DRC) calculations have been carried out on this transition state to estimate the inner-sphere freqencies which carry the system through the transition state. In the DRC calculation the geometry constraints which force **[22/HEX/22]**$^{+\ddagger}$ to have the same dinitrogen unit geometries are removed. At time 0, the molecule has only potential energy, but vibrations are activated which would carry it to relaxed **[22/HEX/22]**$^+$ if its excess energy could be dissipated. This excess energy cannot be dissappated in the calculations, so the molecule oscillates, swapping energy back and forth between potential and kinetic energy (PE and KE) as a function of time. DRC enthalpies were calculated every 0.1 fs for 2.39 ps. The KE (or PE) versus time curve contains information on the frequencies which are activated by allowing the geometry to relax from the transition state. The KE(t) curve for **[B/TET/B]**$^{+\ddagger}$ appears as Figure 3. A KE vs t plot may be described as a free induction decay, from which the frequency, intensity information $I(h\nu)$ may be recovered by carrying out a Fourier transform (FT). The frequencies obtained by the FT must be divided by 2 because the momentum P of a harmonic oscillator of frequency ω is proportional to $\sin(\omega t)$, and the total energy $K = P^2/2M$, so K is proportional to $[1 - \cos(2\omega t)]$. The fast Fourier transform (FFT) algorithm used for the calculation requires the use of a data set having 2^n points, and produces

(10) Rauhut, G.; Clark, T. *J. Chem. Soc., Faraday Trans.* **1994**, *90*, 1783.
(11) (a) Doorn, S. K.; Hupp, J. T. *J. Am. Chem. Soc.* **1989**, *111*, 1142. (b) Doorn, S. K.; Hupp, J. T. *J. Am. Chem. Soc.* **1989**, *111*, 4704. (c) Doorn, S. K.; Hupp, J. T.; Porterfield, D. R.; Campion, A.; Chase, D. B. *J. Am. Chem. Soc.* **1990**, *112*, 4999. (d) Blackbourn, R. L.; Johnson, C. S.; Hupp, J. T.; Bryant, M. A.; Sobocinski, R. L.; Pemberton, J. E. *J. Phys. Chem.* **1991**, *95*, 10535. (e) Doorn, S. K.; Blackbourn, R. L.; Johnson, C. S.; Hupp, J. T. *Electrochim. Acta* **1991**, *36*, 1775.

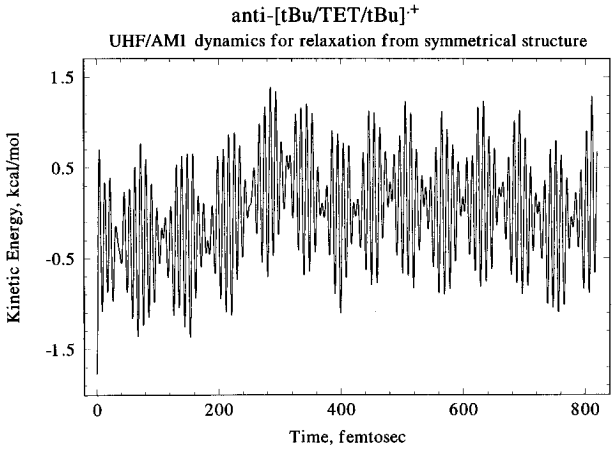

Figure 3. KE vs time for DRC calculations on **s[B/TET/B]**$^+$ followed for two[13] 0.1-fs increments.

intensities as a function of frequency, with a channel width $\Delta h\nu$ of $1/(2 \times c \times \Delta T)$, where the time the data set covers is $\Delta T = 0.1 \times 10^{-15}$ s $\times$ (number of points). Thus following the DRC for 2^{12} points ($\Delta T = 409.6$ fs) makes the $\Delta h\nu$ channels 40.72 cm^{-1} wide, 2^{13} points ($\Delta T = 819.2$ fs) 20.36 cm^{-1}, and 2^{14} points ($\Delta T = 1638.4$ fs) 10.18 cm^{-1}. The average KE was subtracted from the KE(t) points in the "FID", which makes KE_{av} oscillate about zero at long times (this was done before plotting Figure 3). This removes an arbitrary, large calculated intensity at $h\nu = 0$ in the $I(h\nu)$ file. Figure 4 shows the $I(h\nu)$ plots produced for **[22/HEX/22]**$^{+\ddagger}$ using the 10^{13} points at the beginning, middle, and end of the 2.39 ps data set. It will be noted that the relative intensities depend upon time. At longer times the bands are more uniformly distributed, and frequencies which are essentially absent in the first 2^{13} point plot have large intensities in the last plot. Following the DRC long enough to give good resolution distorts knowledge of which frequencies are activated at the transition state because vibrational energy is increasingly distributed into other modes as time increases.

To more accurately estimate the initially activated vibrations, we have used "Gaussian apodization". The $KE_{av}(t)$ file was multiplied by $f(i) = \exp(-T^2W^2\pi)$, where T is the time (in 0.1 fs units) and W is varied. This keeps the same number of channels in the $I(h\nu)$ files, but the real resolution goes down as the effective time followed is decreased, which makes intensity "spill" into adjacent channels. The time at which $f(i)$ is $1/e$th that at $t = 0$, τ', and the effective band width, $\Delta h\nu' = 1/(2 \times c \times \tau')$, are summarized in Table 2. Resolution increases as τ' increases, but the relative intensities are altered significantly at long times. Figure 5 compares the 150- and 350-fs files, showing that the bands are more fully resolved at 350 fs, and that the intensities are not too different. Obtaining the desired initial $I(h\nu)$ distribution is only approximate because the effective band width increases as τ' decreases, and we estimated them using a plot of the relative $I(h\nu)$ vs τ' (see supporting information). The 611-cm^{-1} band clearly has anomalously large intensity at short τ' because it starts overlapping significantly with the larger 672-cm^{-1} band, and their overlap at small τ' will increase the relative intensities for the 1211- and 1354-cm^{-1} bands. We suggest that the increases in intensity relative to the 672-cm^{-1} band for 71-, 143-, 539-, and 1456-cm^{-1} bands and the decrease for the 1720-cm^{-1} bands are probably caused by vibrational equilibration at longer times, and estimate the initial intensities as summarized in the second column of Table 3.

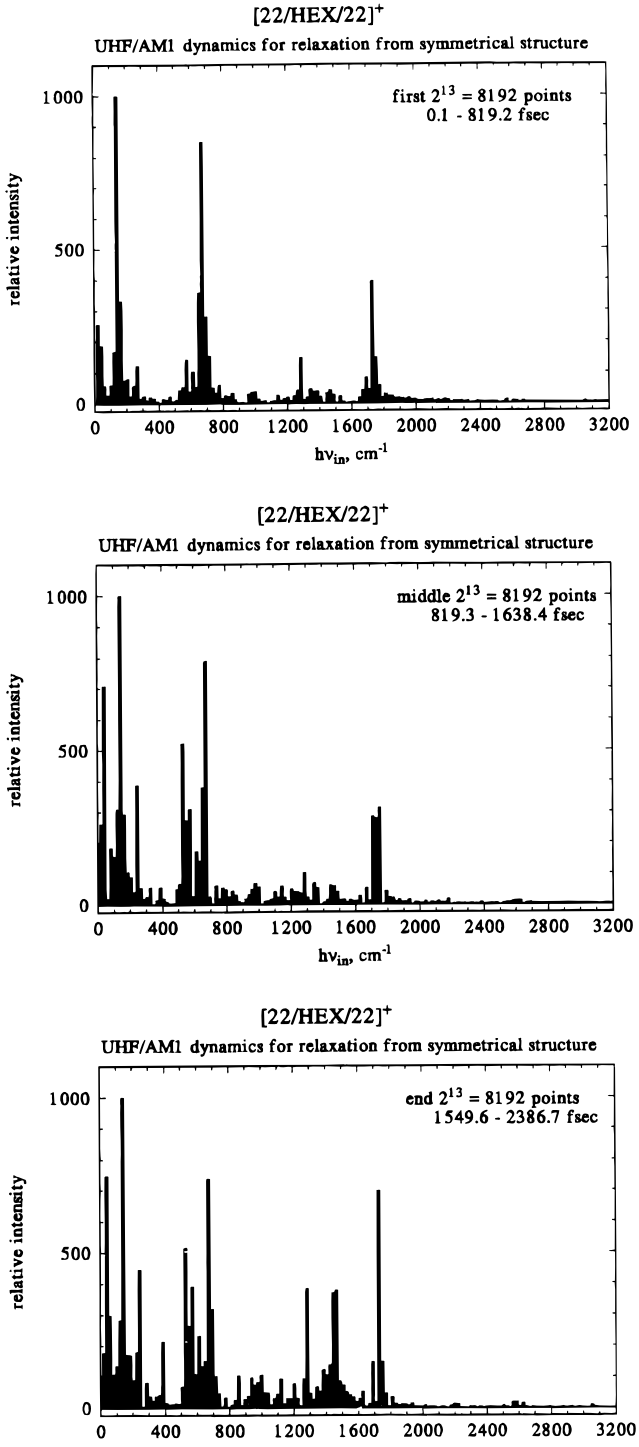

Figure 4. $I(h\nu)$ plots from Fourier tranformed KE_{av} vs time data for **[22/HEX/22]**$^{+\ddagger}$ from the initial, middle, and final 2^{13} points from DRC calculations over 2.39 ps.

Vibrational energy calculations cannot be carried out on the transition states because they have large gradients when the geometry constraints forcing the nitrogens to be equivalent are removed. This demonstrates that UHF/AM1 calculations do not get the C_{2v} **[22/HEX/22]**$^{+\ddagger}$ structure to be a transition state

(12) Nelsen, S. F.; Wang, Y. *J. Org. Chem.* **1994**, *59*, 1655.

(13) (a) Hupp and Dong[13b] have recently used expression 1a suggesting that (3) makes the observed transition energy different from λ. E_{op}', however,

$$E_{op}' = (\lambda^2 + 4V^2)^{1/2} \quad (1a)$$

represents the surface separation at $X = 0$, the minimum for the diabatic surface. The mixing in (3) moves the minimum slightly, which has a large effect on the surface separation. For $\lambda = 46.6$, $V = 5.0$ kcal/mol, (1a) gives $E_{op}' = 47.66$ kcal/mol, but the minimum on the ground state surface occurs at 0.011_7, where the surface separation is indeed equal to λ (Figure 7). (b) Hupp, J. T.; Dong, Y. *J. Am. Chem. Soc.* **1993**, *115*, 6428.

(14) Jortner, J.; Bixon, M. *J. Chem. Phys.* **1988**, *88*, 167.

Table 2. Dependence of the Effective Resolution $\Delta h\nu'$ on the Mean Lifetime τ' Introduced by Multiplying the $KE_{av}(t)$ Values by $f(i) = \exp(-T^2W^2\pi)$

10^4W	τ' (fs)	$\Delta h\nu'$ (cm^{-1})
0.7525	750.0	22
1.000	564.2	30
1.612	350.0	48
2.000	282.1	59
2.357	250.0	67
3.761	150.0	111
5.000	112.8	148

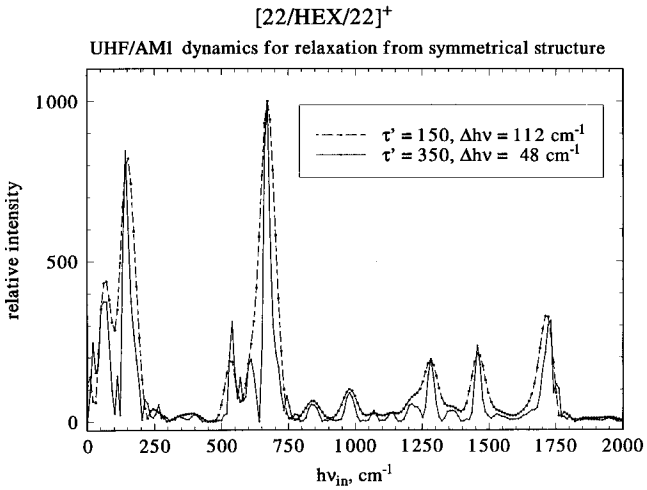

Figure 5. Comparison of intensity, $h\nu_{in}$ plots for **[22/HEX/22]**$^{+\ddagger}$ using Gaussian apodization at $\tau' = 150$ and 350 fs.

for any nuclear motion. We nevertheless believe that it is the UHF/AM1 transition state for electron transfer as defined by Marcus,[3] where the geometries of the units undergoing ET are the same, so the odd electron can be on either one. Association of the frequencies found to be activated at the ET transition state by the DRC calculation with molecular motions can be carried out by AM1 calculations on relaxed (C_s) **[22/HEX/22]**$^+$ and the monomer units **22/22^0** and **22/22**$^+$. Raman bands identified as having the significant NN stretches (S) and nitrogen pyramidality changes (F for flap angle) which are expected to be important for attaining the ET transition state have been included in Table 3, along with their qualitative relative motion (F,FF,FFF for small movement to large). The modes for relaxed dimer are often more complex and harder to describe. We describe them qualitatively in Table 3 using regions in which the principal atom motions occur, using the abbreviations shown using the side and top views of the molecule as shown below.

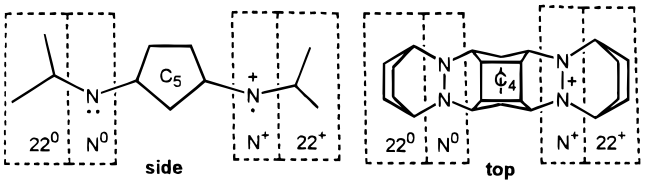

All modes indicated as being important by the DRC involve nitrogen pyramidality changes or NN stretching, and all are found at very similar frequencies in the normal mode calculation for relaxed **[22/HEX/22]**$^+$ (see supporting information). Not surprisingly, the intensities derived from the DRC are very different from those for the Raman spectrum calculation. Modes involving NN twist and CN stretch do not appear in the DRC, suggesting that they are unimportant, presumably because neither quantity is very different for the neutral and radical cation oxidation states of **22/22**. The modes below 850 cm^{-1} are dominated by pyramidality changes, and those above 1050 cm^{-1} by stretching frequencies. The greater complexity of the 933−955-, 1070−1098-, and 1200−1209-cm^{-1} regions of **[22/HEX/22]**$^+$ indicate that these regions of the transition state DRC contain overlapping bands. Many vibrational modes are clearly activated in achieving the ET transition state for **[22/HEX/22]**$^+$, and the individual modes of the two oxidation states appear, not their averages. A qualitatively similar picture for other systems has been obtained experimentally, especially by the resonance Raman work of Hupp's group.[11]

These DRC calculations give the result that 77% of λ_{in} for **[22/HEX/22]**$^+$ (∼29 kcal/mol) is caused by modes with frequencies under 1000 cm^{-1}, principally pyramidality changes. About 12% of λ_{in} (4.5 kcal/mol) is estimated to arise from the two main NN stretching modes, with a slightly greater contribution from the 1720-cm^{-1} N^+ stretch than from the 1456-cm^{-1} N^0 stretch. It appears clear that the unusually large λ_{in} values for hydrazines have very large low-frequency nitrogen bending contributions. Nevertheless, we do not doubt that AM1 calculations will overemphasize bending relative to stretching modes

Table 3. Estimates of Initial Vibrationally Activated Modes for **[22/HEX/22]**$^{+\ddagger}$ and Comparison with Modes of Relaxed (C_s) **[22/HEX/22]**$^+$ and the "Monomers"

[22/HEX/22]$^{+\ddagger}$		**[22/HEX/22]**$^+$	**[22/22]**^{0}	**[22/22]**$^+$
$h\nu$ (cm^{-1})	est I_{in}[a]	$h\nu$(assig) (cm^{-1})	$h\nu$(assig)[b] (cm^{-1})	$h\nu$(assig)[b] (cm^{-1})
71	0.45 (0.42)	51 (F[N^+])		98(FF)
143	0.84 (0.82)	145 (F[N^0/N^+])	215 (F)	
			398 (F)	
539	0.13 (0.26)	537 (FF[$22^0N^+C_5N^+22^+$])		576(FF)
611	0.21 (0.21)	608 (FFF[N^+22^+])	609 (FFF)	
672	1.00 (1.00)	670 (FFF[22^0N^0])	708 (FFF)	656 (FFF)
844	0.05 (0.06)	824 (F[N^+22^+])[c]	867 (F)	836 (F)
		828 (F[22^0N^0])[c]		
977	0.09 (0.10)	933, 942, 972, 995[d]	974 (SS/F)	957 (SS/F)
1069	0.03 (0.03)	1070 (S[C_5])		
		1092, 1098 (S[C_5])	1103 (S)	
1140	0.05 (0.03)	1140 (S[22^+22^0])	1125 (SS), 1167 (S)	1135 (S)
1211	0.08 (0.06)	1205, 1209 (S[N^022^0])	1214 (SS), 1219 (SS)	
		1200 (S[N^022^0])		
1283	0.20 (0.19)	1287 (S[N^+22^+])	1284 (SS/F)	1272 (S/F), 1281 (SS)
1354	0.05 (0.04)	1369 (S[$C_4N^{0,+}$])	1369 (S), 1393 (S)	
1456	0.18 (0.22)	1455 (SSS[N^0])	1449 (SSS), 1464 (S)	
1720	0.25 (0.34)	1723 (SSS[N^+])		1716 (SSS)

[a] Estimated initial intensity relative to the 672-cm^{-1} band. The numbers in parentheses are I at $\tau' = 250$ fs, where $\Delta h\nu'$ is 67 cm^{-1}. [b] All of the bands have A_1 symmetry. [c] Principally CH_2 rock. [d] All are SS/F[C_5], variously coupled to N^0 and N^+ and both.

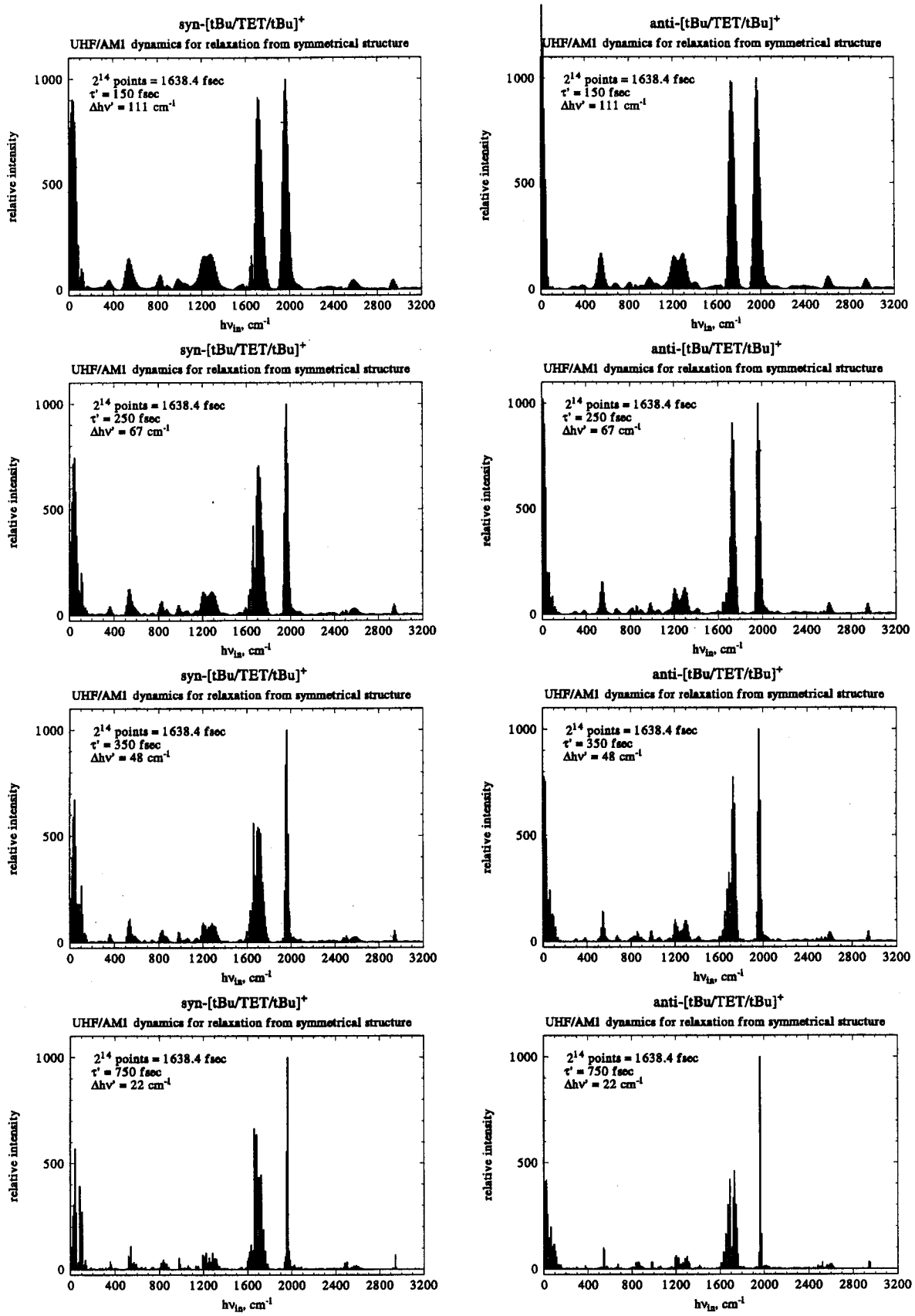

Figure 6. $I(h\nu)$ plots for syn (left column) and anti (right column) **[B/TET/B]**$^{+\ddagger}$ followed for 1.64 ps, using Gaussian apodization to 150, 250, 350, and 750 fs.

for these systems because they get the NN bond length in the neutral hydrazine significantly too short[7] and also calculate inversion barriers at nitrogen which are too high. How large the errors introduced by shortcomings in the AM1 geometries really are is impossible to estimate at this time. Rauhut and Clark's DRC calculations found pyramidalization changes to also be quite important for tetramethyl-p-phenylenediamine ET.[10]

Dynamics calculations as outlined above were also carried out on **s-** and **a[B/TET/B]**$^{+}$ (see supporting information). Figure 6 shows the changes in the $I(h\nu_{in})$ plots calculated as τ'

is increased, demonstrating that rather rapid loss of intensity at very low frequency and at the N^0 stretching frequency is especially apparent for these cases. We presume that the rather small bands above 2000 cm^{-1} visible in Figure 6 (similar bands are less distinct but obviously present for the bis(hydrazine) in Figure 5) are combination bands. Less intense overtones are calculated at twice the N^+ and N^0 stretching frequencies (this region is not shown in Figure 6). The 3e$-\pi$ bond NN stretching modes are calculated to have nearly the same energy for the hydrazines (N^+) and the diazeniums (N^0). NN stretching frequencies are clearly much more dominant in the calculations for the bis(diazeniums) than for the bis(hydrazine). For syn and anti **[B/TET/B]**$^+$ 54 and 46% of λ_{in} (10.0 and 7.9 kcal/mol) is estimated to arise from the N^+ and N^0 stretches, respectively, so not only is the NN stretching contribution relatively larger, but its magnitude for **[B/TET/B]**$^+$ is roughly twice the 4.5 kcal/mol estimated for hydrazine **[22/HEX/22]**$^+$. The AM1-calculated difference in bond lengths for the two oxidation states of diazenium **22/B** (0.070 Å) is slightly smaller than that for **22/22** (0.084 Å), so we presume that the higher stretching frequency for the $(N{=}N)^+$ bond of the oxidized diazenium than for the $(N{-}N)^+$ bond of the oxidized hydrazine (1964 and 1720 cm^{-1}) is responsible for the larger increment in λ_{in}. The nitrogens are nearly planar even in the neutral hydrazyl unit of **[B/TET/B]**$^+$, and few bands identified as bending modes at nitrogen of the monomers and relaxed dimers are found to be important in the dynamics calculation (see supporting information). Although bending modes are far less important than for the hydrazine, the lowest frequency mode at 31 and 10 cm^{-1} respectively is predicted to contribute 29 and 41% of λ_{in} (5.4 and 7.0 kcal/mol, respectively). Because these modes are predicted to lose their energy to other modes rather rapidly, it seems possible that their calculated importance might have been underestimated because of the τ' resolution problem. We do not know how to assign the 31- and 10-cm^{-1} modes for syn and anti **[B/TET/B]**$^+$, although the N^0 bend is an obvious candidate. We have no way of knowing if the large intensity of these bands is some sort of an artifact in the calculation. We would have expected smaller differences between the syn and anti bis(diazeniums) than were obtained in the DRC calculations. The differences found might principally reflect errors in the way we estimate initial λ_{in}(q) values, which is obviously qualitative.

AM1 calculations are known not to be extremely accurate for hydrazines. They seriously underestimate the NN^0 bond length and incorrectly get the bicyclo[2.2.2]octyl rings untwisted in for **[22/22]^0**.[7] Nevertheless, AM1 calculations appear superior to the far more computationally expensive UHF/6-31G* *ab initio* calculations for the purpose of calculating λ_{in}. Although *ab initio* calculations get much better **[22/22]^0** NN bond lengths and twist, they get **[22/22]**$^+$ far too planar and presumably as a result (see Figure 1) overestimate λ_{in} by about 50%. Of course the principal advantage of AM1 calculations is that they are rapid enough to allow dynamics studies in reasonable periods of time. Several dozen hours of Stardent 3000 cpu time are required for the calculations reported here (although we managed to expend several hundreds of hours figuring out how to optimize the initial structures and what to do then). Comparable calculations at the 6-31G* level would require too much time to be practical and would not be expected to give as good results because they get λ_{in} seriously in error.

Studies of ring size effects on k_{ex} for self-ET of *N*,*N*′-bisbicyclic hydrazines indicate that AM1 calculations underestimate λ_{in} for **[22/22]$^{0/+}$** by about 8 kcal/mol,[12] presumably because they get the bicyclic rings of **[22/22]^0** untwisted, while they actually are twisted 13°. This error is probably minimized by choosing the rigid HEX linker for the bis(hydrazine), which probably allows less twist at the neutral NN unit of **[22/HEX/22]**$^+$. The AM1 calculations get close to the experimental values of λ_{in} for both **[22/HEX/22]**$^+$ and **[B/TET/B]**$^+$. They may be doing so "for the wrong reason", which could skew the dynamics results in ways that are difficult to estimate accurately. Although neither the $\lambda_{in}(q)$ values nor the $h\nu_{in}(q)$ values are very accurate, they provide a reasonable starting point for considering a multiple mode analysis, which we feel is necessary to understand ET in these compounds.

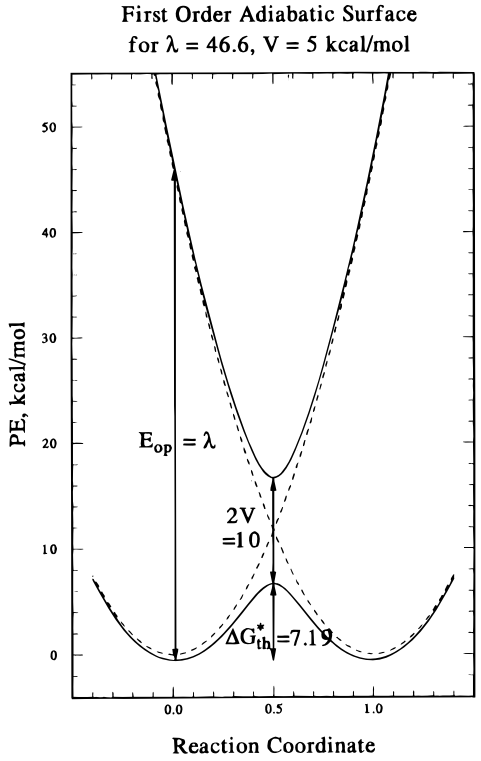

Figure 7. First-order adiabatic energy surface calculations using (3) for the λ and V of **[22/HEX/22]**$^+$. The diabatic wells are shown as dotted lines.

Estimation of *V* from AM1 Calculations

For energy surfaces constrained to be parabolas, the electronic matrix coupling element V is the energy difference between the curve crossover point (λ/4) and the transition state energy. The enthalpy of the crossover point of the precursor and product energy curves should occur at λ'/4, and the difference between the transition state enthalpy and that of the relaxed ground state is $\Delta H_f([]^{+\ddagger}) - \Delta H_f([]^+)$. However, $\lambda'/4 - [\Delta H_f([]^{+\ddagger}) - \Delta H_f([]^+)]$ for bis(diazenes) is only 0.7−1.1 kcal/mol for the three systems studied, as pointed out previously.[4] This is significantly less than current estimates for V through four aligned σ bonds.[2c] Because energy curves are not quite parabolas and the ET transition state occurs far from the bottom of the well, where non-harmonic deviations are possibly significant, this method might be expected to be risky, and from the calculations discussed below, it is clear that using the above approximation does not predict the AM1-calculated V for these molecules.

V is half the energy difference between the ground and excited state energy surfaces at the transition state. A single SCF calculation at the symmetrical "transition state" geometry without using the density file from the fully optimized transition state calculation produces the first excited state for all three of the symmetrical "ET transition states" discussed here. The excited state for **[22/HEX/22]**$^{+\ddagger}$ lies 12.25 kcal/mol higher in

Table 4. Data for Estimation of $\langle h\nu_{in}\rangle$ and $\langle\Gamma\rangle$ from DRC Calculations on **[22/HEX/22]**$^{+\ddagger}$

q	$\nu_{in}(q)$ (cm^{-1})	Fr[a]	$\lambda_{in}(q)$[b] (kcal/mol)	$\Gamma'(q)$ (300K)[c]	$\Gamma''(q)$ (300K)[d]
1	672	0.277	10.42	2.12	2.59
2	143	0.233	8.75	1.04	1.05
3	71	0.125	4.69	1.01	1.01
4	1720	0.069	2.60	1.79	4.89
5	611	0.058	2.19	1.15	1.35
6	1283	0.055	2.08	1.43	2.68
7	1456	0.050	1.88	1.44	3.11
8	539	0.036	1.35	1.07	1.22
9	977	0.025	0.94	1.12	1.67
10	1211	0.022	0.83	1.14	2.02
11	844	0.014	0.52	1.05	1.43
12	1354	0.014	0.52	1.10	2.18
13	1140	0.014	0.52	1.08	1.81
14	1069	0.008	0.31	1.04	1.66

[a] Fr $= \lambda_{in}(q)/\lambda_{in}$, estimated from intensities in the DRC analysis (Table 3, column 2). [b] Using the experimental λ_{in} of 37.6 kcal/mol. From eq 2, $\langle h\nu_{in}\rangle = 827$ cm^{-1}. [c] From eq 3. Using eq 4, $\langle\Gamma'(300K)\rangle = 16.6$. [d] From eq 6. Using eq 4, $\langle\Gamma''(300K)\rangle = 5.80 \times 10^3$.

energy, so this UHF/AM1 calculation gives $V = 6.12$ kcal/mol. The **[B/TET/B]**$^{+\ddagger}$ isomers behave similarly, producing $V = 5.22$ and 5.40 kcal/mol for the syn and anti isomers, respectively. These numbers are far closer to what people are estimating for V in such systems.[2c] Hush theory analysis of the optical bands produces $V = 3.5 \pm 0.5$ for the seven dimeric 4-σ-bond linked **TET** and **HEX** NN radical cations studied,[4,5] which is significantly smaller than those obtained by the above procedure.

Estimation of ET Parameters for [22/HEX/22]$^+$ and Comparison with Theory

Table 4 shows the $\lambda_{in}(q)$ contributions to λ_{in} associated with each of the 14 modes obtained from the DRC on **[22/HEX/22]**$^{+\ddagger}$. The effective barrier crossing frequency, $\langle h\nu_{in}\rangle$, calculated using eq 2 (which is eq 45),[3b] is 827 cm^{-1}. This is quite

$$\langle h\nu_{in}\rangle = \left[\sum_q (h\nu_{in}(q))^2\lambda_{in}(q)/\lambda_{in}\right]^{1/2} \quad (2)$$

low compared to the estimates usually used for organic compounds, and arises because of the large calculated importance of low-frequency modes. All evidence suggests that V is > 3 kcal/mol, which makes ν_{el} significantly larger than ν_n, and the ET adiabatic.[3]

The simplest theoretical treatment for adiabatic ET reactions is the first-order PE surface treatment detailed by Sutin (ref 3b, p 455), in which introducing an electronic coupling V mixing the zero-order parabolic diabatic energy surfaces leads to (3),

$$\mathbf{PE}_{\pm} = 0.5\lambda(2X^2 - 2X + 1) \mp 0.5[\lambda^2(2X-1)^2 + 4V^2]^{1/2} \quad (3)$$

which is (34),[3b] for which X is the fractional position on the reaction coordinate of the diabatic surfaces, and has been written for our $\Delta G^\circ = 0$ cases. In this treatment $E_{op} = \lambda$,[13] and the thermal barrier ΔG^*_{th} is given by (4). As shown in the plot of

$$\Delta G^*_{th} = \lambda/4 - V + V^2/\lambda \quad (4)$$

(3) for the **[22/HEX/22]**$^+$ λ and estimated V (Figure 7), ΔG^*_{th} is 7.2 kcal/mol, only 62% of $\lambda/4$ for this system and surprisingly close to the 7.9 kcal/mol obtained by AM1 calculations. Using (5) as the rate constant predicted by this first-order PE surface

$$k_{ex}(1\text{st order}) = c\langle h\nu_{in}\rangle(\lambda_{in}/\lambda)^{1/2}\exp(-\Delta G^*_{th}/RT) \quad (5)$$

treatment, the observed $k_{ex}(300)$ and λ gives a V which is almost independent of $\langle h\nu_{in}\rangle$ because tunneling is not considered, 4.95 $\pm$ 0.15 for $\langle h\nu_{in}\rangle$ between 800 and 1200 cm^{-1} (Figure 8).

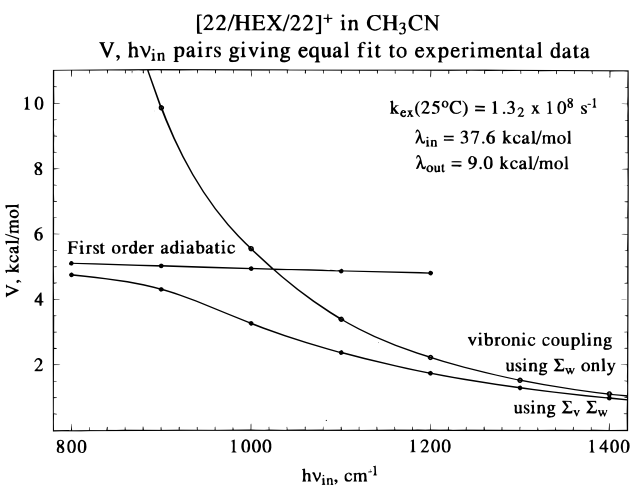

Figure 8. Comparison of equally good fit V vs $h\nu_{in}$ curves for the experimental data of **[22/HEX/22]**$^+$ using the first-order adiabatic eq 5, the $\Sigma_v\Sigma_w$ vibronic coupling eq 6, and the Σ_w only "golden rule" vibronic coupling equations.

Vibronic coupling treatments including tunneling such as that discussed by Jortner and Bixon[14] are obviously far more sophisticated. We will use the single averaged vibrational mode treatment usually employed. The form of this treatment called the "golden rule" by Closs and Miller[15c] considered only excitations in the product well. This is appropriate for the inverted region, but not for the $\Delta G^\circ = 0$ case we are considering, where excitations in the initial and product wells must be of equal importance. The proper form for use in our work is (6),[16] where the vibronic coupling factor $S = \lambda_{in}/h\nu_{in}$.

$$k_{ex} = 2\pi^{3/2}/h(RT)^{1/2}\cdot[V^2/(\lambda_{out})^{1/2}]\cdot(\text{SUMS}) \quad (6a)$$

$$\text{SUMS} = \left[\sum_v \exp(-vh\nu_{in}/RT)\right]^{-1}\cdot\sum_v\sum_w F(v,w)\times \exp(-vh\nu_{in}/RT)\exp[-(\lambda_{out} + \{v-w\}h\nu_{in})^2/4\lambda_{out}RT] \quad (6b)$$

$$F(v,w) = \exp(-S)v!w!\times \left[\sum_r \{(-1)^{v+w-r}S^{(v+w-2r)/2}\}\Big/\{r!(v-r)!(w-r)!\}\right]^2 \quad (6c)$$

The sums are over v and $w = 0$ to ∞. $F(v,w)$ is the Franck–Condon factor for v–w coupling, and the sum is from $r = 0$ to the minimum of v and w. We have not seen it pointed out that (6) converges especially rapidly as ΔG° approaches zero; it is 99% that of the final value by $v, w = 2$ for our data. We have chosen to write (6) in a slightly non-traditional form to emphasize its relationship to the equations including tunneling used by Marcus and Sutin.[3] We transferred the factor $(4\pi\lambda_s k_B T)^{-1/2}$ from FWCD to the first terms in (6a) and we renamed what remains SUMS, which makes it easier to see that k_{ex} contains the electronic coupling factor $\nu_{el} = 2\pi^{3/2}/h(RT)^{1/2}\cdot[V^2/(\lambda_{out})^{1/2}]$ (eqs 37–38),[3b] which is the preexponential term used in diabatic ET equations,[3] and that the $v, w = 0$ exponential term of SUMS is the same as Holstein's κ_n (eq 70[3b]) except that this equation contains a tanh($h\nu_{in}$/4RT) factor, which is ≥

(15) (a) Liang, N.; Miller, J. R.; Closs, G. L. *J. Chem. Phys.* **1989**, *111*, 8740. (b) Liang, N.; Miller, J. R.; Closs, G. L. *J. Am. Chem. Soc.* **1990**, *112*, 5353. (c) Closs, G. L.; Miller, J. R. *Science* **1988**, *240*, 440.

(16) (a) Ulstrup, J.; Jortner, J. *J. Chem. Phys.* **1975**, *63*, 4358. (b) Jortner, J. *J. Chem. Phys.* **1976**, *64*, 4860. (c) We thank Joshua Jortner for pointing this out to us.

Table 5. Calculated Effective Frequencies, Tunneling Factors, and Rate Constants Using Eqs 7−10

$h\nu_{in}$[a]	λ[b]	λ_{in}[c]	T (K)	$\langle\Gamma'\rangle$	k'_{ex} (s^{-1})	R'[e]	$\langle\Gamma''\rangle$	k''_{ex} (s^{-1})	R''[f]
				[22/HEX/22]$^{+‡}$					
827	46.6	37.6[f]	250	63.3	9.22×10^4		1.72×10^5	2.50×10^8	
			300	16.6	1.21×10^6		5.80×10^3	4.21×10^8	
			350	7.28	8.62×10^6	93	6.57×10^2	7.78×10^8	3.1
				s[B/TET/B]$^{+‡}$					
1403	26.9	17.9[g]	200	151	2.32×10^8		3.29×10^6	5.07×10^{12}	
			250	34.3	1.56×10^9		4.06×10^4	1.84×10^{12}	
			300	13.3	5.76×10^9		2.60×10^3	1.13×10^{12}	
			350	6.99	1.52×10^{10}	9.7	4.14×10^2	8.98×10^{11}	0.49
				a[B/TET/B]$^{+‡}$					
1293	26.4	17.4[g]	250	18.0	9.65×10^8		4.10×10^4	2.19×10^{12}	
			300	8.32	4.07×10^9		2.64×10^3	1.29×10^{12}	
			350	4.93	1.17×10^{10}	12.1	4.23×10^2	1.01×10^{12}	0.46

[a] $\langle h\nu_{in}\rangle$ in cm^{-1} from the DRC calculation. [b] kcal/mol, using observed E_{op} values at 298 K in acetonitrile. [c] kcal/mol. [d] $R' = k_{ex}'(350K)/k_{ex}'(250K)$. [e] $R'' = k_{ex}''(350K)/k_{ex}''(250K)$. [f] Using the solvent dependence of E_{op}, which gives $\lambda_{out}(CH_3CN) = 9.0$ kcal/mol.[5] [g] Assuming λ_{out} is the same as for **[22/HEX/22]$^+$**. It should be noted that λ was estimated from the CT band maximum, and not using the shoulder, which as pointed out in the text would probably be more appropriate. This would make the k_{ex} estimates even larger.

0.86 at $h\nu_{in} \geq 1000$ cm^{-1}. Figure 8 shows plots of equivalent fits for (6) and the $\sum_w$ only ("golden rule") equation to the experimental $k_{ex}(300)$ and λ values of **[22/HEX/22]$^+$**. It may be seen that the $\sum_w$ only form is equivalent to (6) at $h\nu_{in}$ above about 1300 cm^{-1}, which allowed Liang, Miller, and Closs to use it even for their small $\Delta G°$ cases[15a] (they used $\langle h\nu_{in}\rangle =$ 1500 cm^{-1} for all of their compounds). The equations diverge greatly at smaller $\langle h\nu_{in}\rangle$, and for the 827 cm^{-1} obtained from the DRC calculations, the V using (6) is 4.74 kcal/mol, while that using the $\sum_w$ only form is 16.01, which is unreasonably large.[2c] The V obtained using (6) is surprisingly close to the 5.0 obtained using (5), see Figure 8, and is between the 3.9 obtained from a Hush treatment of the optical band intensity, width, and position and the 6.1 calculated by AM1. Using values of $\langle h\nu_{in}\rangle$ above 1030 cm^{-1} would make the V obtained under 3 kcal/mol, so the small $\langle h\nu_{in}\rangle$ obtained by the DRC is also suggested from the observed rate constant and λ when used with (6). Although we consider the agreement of (5) and (6) with the experimental $k_{ex}(300)$ to be surprisingly good, there is still a serious problem, because both fail to predict the small $k_{ex}(350)/k_{ex}(250)$ ratio which is observed. Equation 5 gives a ratio of 62, and (6) a ratio of 81.

We shall now try to consider whether a multiple mode analysis, which the DRC calculations suggest ought to be necessary, improves the fit to experiment. It can be noted from Table 4 that although three-quarters of the barrier is calculated to be caused by modes with frequencies under 1000 cm^{-1}, several higher frequency modes also contribute. Each mode will have a different tunneling factor $\Gamma(q)$, and these are also summarized in Table 4. Sutin (ref 3b, p 468) discusses semiclassical theories in which nuclear tunneling through the $\lambda_{in}(q)$ barriers is considered. Very different results are obtained depending upon which literature expression is chosen for $\Gamma(q)$ (see Table 5). Holstein's[17] expression for $\Gamma(q)$, which we shall call $\Gamma'(q)$, is (7)

$$\Gamma'(q) = \exp\{-S[\tanh(F) - (F)]\} \quad (7)$$

(quoted by Sutin as eq 69),[3b] and has been written using the abbreviations $S = \lambda_{in}(q)/h\nu_{in}(q)$ and $F = h\nu_{in}(q)/4RT$. The effective value of the nuclear tunneling factor is given by eq 8

$$\langle\Gamma\rangle = \prod_q \Gamma(q) \quad (8)$$

(eq 12).[2c] We shall call $\langle\Gamma\rangle$ values estimated using Holstein $\Gamma'(q)$ values $\langle\Gamma'\rangle$. The ET rate constant ought to be estimable using eq 9. Using the experimental λ_{in} and λ values for **[22/HEX/22]$^+$**

$$k_{ex}(\text{ad}) = c\langle h\nu_{in}\rangle(\lambda_{in}/\lambda)^{1/2}\langle\Gamma\rangle \exp(-\lambda/4RT) \quad (9)$$

with the $\langle h\nu_{in}\rangle$ and $\langle\Gamma'\rangle$ values gives $k_{ex}(300) = 1.20 \times 10^6$ s^{-1}, a factor of 110 smaller than experiment, and a rate ratio $k_{ex}(350)/k_{ex}(250)$ of 94, far larger than the 2.0 observed. Something is significantly wrong with using (9) with $\langle\Gamma'\rangle$ for the **[22/HEX/22]$^+$** data.[18] The Jortner expression (6), which treats vibronic coupling similarly but explicitly includes V in the rate equation, gives much better agreement with $k_{ex}(300)$, but only includes one averaged mode. Even if a multiple mode version of (6) were properly implemented, it could not give a $k_{ex}(350)/k_{ex}(250)$ rate ratio below about 5 because of the form used for the temperature dependencies.[16c]

The conformational complexity of **[22/HEX/22]$^+$** might somehow be involved in the low observed temperature sensitivity of k_{ex}; we have assumed the ET occurs within **oo**, but this might be wrong. We are unable to think of a reasonable way that this conformational complexity could cause the anomalously small temperature effect on k_{ex} which is observed. We suggest that something more fundamental may be involved, because use of Hush's tunneling factor gives much better agreement with our data. Hush employs a larger $\Gamma(q)$ than eq 7, instead using eq 10 (eq 10),[2c] where $U(q)$ at 298 K = 1.04 for $h\nu_{in} = 300$

$$\Gamma''(q) = U(q)\Gamma(q) \quad (10a)$$

$$U(q) = (2F\ \text{csch}(2F))^{-1/2} \quad (10b)$$

cm^{-1}, and rises to 2.98 at 1800 cm^{-1}. The individual $U(q)$ values only make $\Gamma''(q)$ slightly larger than $\Gamma'(q)$, but the total value of the nuclear tunneling factor $\langle\Gamma''\rangle$ is far larger than $\langle\Gamma'\rangle$. Hush does not point it out, but use of $\Gamma''(q)$ is very different

(17) (a) Holstein, T. *Philos. Mag. B* **1978**, *37*, 449. (b) Holstein, T. *Tunneling in Biological Systems*; Chance, B., et al., Eds.; Academic: New York, 1979; p 129.

(18) A single mode version of (9) employing $\langle\Gamma'\rangle$ requires $h\nu_{in} = 1395$ cm^{-1} to give the experimental k_{ex} with the experimental λ values. Multiple mode analyses including lower frequencies raise $\langle h\nu_{in}\rangle$. For example, using five equally important frequencies of 71, 143, 672, 1283, and 1456 cm^{-1} with 1720 cm^{-1} requires 70.8% of the barrier (26.6 kcal/mol) to be associated with the 1720 mode, and produces $\langle h\nu_{in}\rangle$ of 1530 cm^{-1}, and using 1456 and 1720 cm^{-1} as equally important and including the other four modes as equally important to each other requires 1456 and 1720 cm^{-1} to each contribute 41.8% of the barrier (15.7 kcal/mol each) and produces $\langle h\nu_{in}\rangle$ of 1487 cm^{-1}.

from use of $\Gamma'(q)$ when multiple modes are considered.[19] Using $\Gamma''(q)$ makes $\langle\Gamma\rangle$ increase simply by including more modes, because $U(q)$ is not affected by the size of $\lambda_{in}(q)$, and appears as a preexponential term. If q modes are included, $\langle\Gamma''\rangle = \langle\Gamma'\rangle\prod_q U(q)$, so the presence of high-frequency modes significantly raises $\langle\Gamma\rangle$ even if $\lambda_{in}(q)$ for the high-frequency modes is small. Use of (10) for evaluation of $\langle\Gamma\rangle$ leads to far better fit to our experimental data. For **[22/HEX/22]**$^+$ using $\langle\Gamma''\rangle$ gives $k_{ex}(300K) = 4.21 \times 10^8\ s^{-1}$, a factor of 3.2 higher than the experimental value, and predicts $k_{ex}(350)/k_{ex}(250) = 3.1$, much closer to the observed value of 2.0. The interesting prediction of a negative activation energy for k_{ex} using $\langle\Gamma''\rangle$ for **[B/TET/B]**$^+$ when many modes are active unfortunately cannot be experimentally tested on these compounds because k_{ex} is (as predicted) too fast to measure by ESR. It is having many modes that causes the $k_{ex}(350)/k_{ex}(250)$ ratio to drop. Using only the 3, 6, and 9 most intense modes of the 11 calculated for **s[B/TET/B]**$^+$ (see supporting information) produces $k_{ex}(350)/k_{ex}(250) = 3.0$, 1.4, and 0.9, respectively.

The use of the $\Gamma''(q)$ values with the $\lambda_{in}(q)$ values obtained from the DRC calculations seems unreasonable. $\Gamma''(q)\exp(-\lambda_{in}(q)/4RT)$ is >1 for the nine modes at 844 cm^{-1} and higher, so the use of $\langle\Gamma''\rangle$ for all of the higher frequency modes appears to have a larger rate-enhancing effect than simply assuming complete tunneling through the higher frequency modes, that is, ignoring their contribution to λ_{in}. However, when only the five lowest frequency modes are assigned as contributing to the effective λ_{in} barrier, and $\langle\lambda_{in}\rangle = 27.39$ kcal/mol is employed, use of $\Gamma''(q)$ for these modes produces $\langle\Gamma''(T\text{K})\rangle$ values of 10.03(250), 4.51(300), and 1.77(350). Using these values in (9) and replacing λ_{in} by $\langle\lambda_{in}\rangle$ then gives $k_{ex}(\text{ad})(T\text{K}) = 1.97 \times 10^8(250)$, $8.79 \times 10^8(300)$, $1.78 \times 10^9(350)$, or a k_{ex}(ad) at 300 K which is 6.7 times that observed, and $k_{ex}(350)/k_{ex}(250) = 9.0$, considerably larger than the observed value of 2. Unreasonable-seeming use of $\Gamma''(q)$ with the entire range of $\lambda_{in}(q)$ values unquestionably fits the experimental data for **[22/HEX/22]**$^+$ better. Tunneling in this system appears to be even more important than that assigned assuming the $\Gamma''(q)$ values only for the lower frequency modes and that tunneling is complete for the higher frequency modes. This sort of analysis obviously cannot determine what tunneling factors really are, but we suggest that it points out that tunneling is apparently more significant for **[22/HEX/22]**$^+$ than would be expected from (7). We have employed both $\Gamma(q)$ expressions far outside the $h\nu_{in} < 2RT$ (414 cm^{-1} at 298 K) range for which they are derived,[2c] as have others who consider tunneling in organic compounds.

Conclusions

UHF/AM1 DRC calculations of the modes activated upon releasing symmetry constraints which hold dimeric intervalence organic compounds at the ET transition state are practical to carry out on molecules the size studied, and indicate that many modes contribute to λ_{in}. We believe that the results that N pyramidality effects dominate for the bis(hydrazine) and NN stretching for the bis(diazenium) ET and that the modes at the transition state are essentially the sum of those for the relaxed units are qualitatively correct, and not something that had been adequately tested previously. AM1 calculations may well overestimate the importance of N pyramidality changes relative to NN bond length changes for hydrazines, and how accurate the AM1 vibrational spectral calculations, and hence the $h\nu_{in}(q)$ values obtained, actually are for these systems remains to be established. The $\lambda_{in}(q)$ values we obtained are probably not quantitatively correct. The observed $k_{ex}(300)$ for **[22/HEX/22]**$^+$ and λ values produce a V near 5 kcal/mol, and the vibronic coupling eq 6 requires a low $\langle h\nu_{in}\rangle$ like that obtained by the DRC to give a similar V. **[22/HEX/22]**$^+$ shows significantly faster ET than the adiabatic k_{ex} expression 9 predicts when used with $\Gamma'(q)$ (7) to estimate $\langle\Gamma\rangle$. The high k_{ex} and small temperature sensitivity for **[22/HEX/22]**$^+$ appear to us to be best explained by a larger tunneling coefficient than (7) predicts. Use of Hush's $\Gamma''(q)$ expression 10 containing a preexponential factor for tunneling gives surprisingly good fit to our data with the simple adiabatic k_{ex} eq 9. It will obviously take further studies to establish whether such analysis proves generally useful.

Table 6. Comparison of Inner-Sphere Parameters for Intervalence Compounds

compd	λ_{in} (kcal/mol)	$\langle h\nu_{in}\rangle$ (cm^{-1})	S[a]
1$^+$	2.0	≤300	2.3
2$^+$	4.7	≤300	5.5
s[B/TET/B]$^+$	17.9	∼1403	4.5
[22/HEX/22]$^+$	37.6	∼827	15.9

The large qualitative difference between using organic molecules and transition metals as the charge and spin-bearing units in intervalence compounds can be seen by the comparison of the inner-sphere ET parameters for our compounds and two well-studied transition metal complexes, **1**$^{+}$[20] and **2**$^+$,[21] shown in Table 6. It is clear that employing organic compounds greatly extends the range of both $h\nu_{in}$ and S studied, which is especially important if tunneling effects are to be understood.

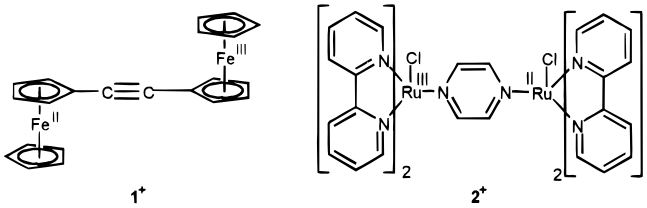

1$^+$ **2**$^+$

We find the DRC results an encouraging indication that $h\nu_{in}(q)$ modes important for ET should be estimable from calculations on the relaxed precursors in the two oxidation states, and therefore that calculations on the dimeric transition states for intermolecular ET reactions should not really be necessary to estimate $h\nu_{in}$ values. Such calculations are quite difficult to carry out, although Clark has done it for one transition state geometry of tetramethyl-*p*-phenylenediamine.[22] We believe that experimental data on phenyl-substituted **22/22** derivative k_{ex} values provides good evidence that many relative orientations are involved in intermolecular ET for hydrazines,[23] which suggests to us that DRC calculations on a single, symmetry-imposed transition state are not likely to be realistic.

Experimental Section

2,7,11,16-Tetraazadecacyclo[15.4.1.2^{3,6}.2^{12,15}.0^{2,7}.0^{8,20}.0^{9,22}.0^{10,19}.0^{18,21}]-hexacosane ([22/HEX/22]) was prepared as previously reported:[5] ^{13}C NMR (90.56 MHz, 230 K, $CDCl_3$) δ 57.84, 54.45, 51.22, 50.94, 42.27, 39.89, 32.96, 29.03, 29.00, 23.36, 22.57.

(19) Hush employs (10) in a single average mode approximation, using $\lambda_{in} = \langle S\rangle\langle h\nu_{in}\rangle$.[2c] Although doing this might not be very different for the $h\nu_{in} < 400\ cm^{-1}$ cases he wanted to consider, it is quite different for our data. Using $\langle h\nu_{in}\rangle = 827\ cm^{-1}$, $\langle S\rangle$ is 15.9, and $\Gamma''(300K) = 55.0$, which is a factor of 105 smaller than $\Gamma''(300K)$ evaluated using (9) and (10); see Table 6.

(20) (a) Powers, M. J.; Meyer, T. J. *J. Am. Chem. Soc.* **1978**, *100*, 4393. (b) McManis, G. E.; Gochev, A.; Nielson, R. M.; Weaver, M. J. *J. Phys. Chem.* **1989**, *93*, 7733. (c) Blackbourn, R. L.; Hupp, J. T. *J. Phys. Chem.* **1990**, *94*, 1788.

(21) Powers, M. J.; Meyer, T. J. *J. Am. Chem. Soc.* **1980**, *102*, 1289.

(22) Rauhut, M.; Clark, T. *J. Am. Chem. Soc.* **1993**, *115*, 9127.

(23) Nelsen, S. F.; Wang, Y.; Hiyashi, R.; Powell, D. C.; Neugebauer, F. A. *J. Org. Chem.* **1995**, *60*, 2981.

AM1 calculations were carried out using VAMP 5.0[24] or earlier versions. We employed the program VISVIB,[25] which reads calculated normal mode vibration output files and displays the motions visually, to locate the atoms showing large motion and assign them to NN stretching, N pyramidalization, or other modes.

Acknowledgment. We thank the National Science Foundation for financial support of this work under grants CHE-9105485 and CHE-9417946. The DRC calculations could not have been done without the instruction of Timothy Clark, who supplied both programs and considerable instruction in their use. His extensive unpublished DRC calculations on **[22/HEX/22]**$^+$ employing RHF/AM1 have also not been discussed. We also thank E. L. Sibert and R. B. Spencer for helpful suggestions on analysis of DRC data, J. T. Hupp and J. Jortner for valuable discussions, and Thomas Preiss for supplying VISVIB. We thank Ling-Jen Chen for doing the ^{13}C-NMR work.

(24) Rauhut, G.; Chandrasekhar, J.; Alex, A.; Steinke, T.; Clark, T. *VAMP 5.0*; Oxford Molecular: Oxford, 1994.

(25) We thank the author of VISVIB, Thomas Preiss, Universität Giessen, for modifying his program to read large VAMP 5.0 files and providing it to us.

Supporting Information Available: Table of estimates of initially vibrationally activated modes for **s[B/TET/B]**$^{+‡}$ and **a[B/TET/B]**$^{+‡}$, compared with assignments for **s[B/TET/B]**$^+$, **a[B/TET/B]**$^+$, **[22/B]**^{0}, and **[22/B]**$^+$ and figures of intensity vs τ' relative to $I = 1000$ for the strongest mode for **[22/HEX/22]**$^{+‡}$ and **[B/TET/B]**$^{+‡}$, comparison of modes and intensities obtained from the DRC on **[22/HEX/22]**$^{+‡}$ with calculated Raman modes for relaxed **[22/HEX/22]**$^+$ which have significant NN distance and pyramidality changes, and comparison of Raman calculations for relaxed **[B/TET/B]**$^+$ with **[B/22]**^{0} and **[B/22]**$^+$ (6 pages). This material is contained in many libraries on microfiche, immediately follows this article in the microfilm version of the journal, can be ordered from the ACS, and can be downloaded from the Internet; see any current masthead page for ordering information and Internet access instructions.

JA952539G